Characteristics of the H-mode Pedestal in Improved Confinement Scenarios in ASDEX Upgrade, DIII-D, JET and JT-60U

C.F. Maggi 1), R.J. Groebner 2), N. Oyama 3), R. Sartori 4), L.D. Horton 1), A.C.C. Sips 1), W. Suttrop 1) and ASDEX Upgrade Team, T. Leonard 2), T.C. Luce 2), M.R. Wade 2) and DIII-D Team, Y. Kamada 3), H. Urano 3) and JT-60U Team, Y. Andrew 5), C. Giroud 5), E. Joffrin 6), E. de la Luna 7) and EFDA-JET Contributors* for the Pedestal and Edge Physics and the Steady State Operation Topical Groups of the ITPA

1) MPI für Plasmaphysik, EURATOM Association, D-85748 Garching, Germany
2) General Atomics, San Diego, California, USA
3) Japan Atomic Energy Agency, 801-1 Mukouyama, Naka-shi, Ibaraki-ken, 311-0193, Japan
4) EFDA Close Support Unit, D-85748 Garching, Germany
5) UKAEA, EURATOM Association, Abingdon, UK
6) CEA, EURATOM Association, Cadarache, France
7) CIEMAT, EURATOM Association, Madrid, Spain

e-mail contact of main author: Costanza.Maggi@ipp.mpg.de

Abstract. Pedestal and global plasma parameters are compared in ELMy H-mode discharges from ASDEX Upgrade (AUG), DIII-D, JET and JT-60U with varying input power and current profiles. Both electron and ion pedestal pressures are studied. The increase in pedestal pressure (p^{PED}) with power is continuous, reflecting the continuous transition from "standard H-mode" to "improved confinement scenario". Higher p^{PED} than in standard H-modes are found in improved H-modes in AUG and in JT-60U high β_{pol} H-modes at $q_{95} = 6.5$. In AUG improved H-modes p^{PED} increases with power due to an increase of both pedestal top density and temperature. In DIII-D p^{PED} increases primarily due to an increase of the pedestal temperature, through an increase in width of the Te ETB and an increase of both width and gradient of the Ti ETB. For AUG the confinement improvement at high input power is due in part to increased core stored energy and in part to increased pedestal stored energy, while in DIII-D hybrid discharges it is due to increased core confinement. In JT-60U high β_{pol} H-modes at $q_{95} = 6.5$ and high δ the improved confinement is due to an increase of W_{PED}, while in reversed shear H-modes to an increase of W_{core}. In JET hybrid discharges at 1.4 MA Wth increases with power and δ due to an increase of W_{PED}. In all four tokamaks improved edge stability is correlated to increasing total β_{pol} and H98(y,2) increases with pedestal β_{pol}.

1. Introduction

The reference scenario for ITER is the standard H-mode with type I ELMs, a confinement factor $H_{98(y,2)} = 1$ and a normalized beta value of $\beta_N = 1.8$. It is designed to reach a fusion gain Q = 10 with pulsed operation lasting for 400 s. A second physics objective for ITER is to demonstrate Q = 5 operation in steady state plasma conditions. As an intermediate step towards this second objective, several tokamaks have developed H-mode scenarios with improved performance, capable in ITER of either Q > 10 or extended pulse duration at lower plasma current. The latter scenario is known as the hybrid scenario. Experiments in present day tokamaks show that one way to achieve this scenario is to modify the q profile of the discharge in such a way as to open access to operation at higher values of β_N. There is evidence that in such discharges the H-mode confinement is higher than in standard scaling laws, at least when compared to the widely used IPB98(y,2) scaling law [1] (the beta and collisionality dependence of this scaling expression are still under investigation [2]). However, the change in confinement from the "conventional" or "standard" H-mode discharges to the improved confinement discharges is continuous and reflects the fact that these discharges occupy different areas (with some overlap) of the operating space of the ELMy H-mode. One important question is how much of this improvement in confinement originates from the pedestal region, since the scaling of the H-

mode pedestal is an open issue when predicting the performance of ITER. In order to answer this question, this paper compares global and pedestal parameters in discharges with varying current profiles and input power from ASDEX Upgrade (AUG), DIII-D, JET and JT-60U. Candidates for improved confinement scenarios for ITER analysed in this paper include the improved H-mode in AUG [3, 4] the hybrid discharges in DIII-D [5], the hybrid discharges in JET [6] and the high-β_{pol} [7] and the reversed shear (RS) ELMy H-modes [8] in JT-60U.

2. Selection of the multimachine database

Conventional H-modes and improved confinement discharges were selected for each tokamak, with the following general criteria: (i) ELMy H-modes with type I ELMs (and some mixed type I/II at high δ for JET); (ii) discharges at safety factors $3 < q_{95} < 6$; (iii) discharges with stationary phases at least 3 energy confinement times long. For each discharge the plasma parameters were averaged over the stationary phase. More specifically, the discharge selection was guided by the emphasis on the study of the variation of the pedestal with input power. For continuity reasons, in this paper the labels "standard H-mode", "hybrid discharge", etc used in the figures are those that had been assigned to the specific plasma discharge at the time it was run during a particular physics session. This "control room" definition can lead to some ambiguity in the region of overlap of the two operating spaces. A more physics based classification could be done in terms of Q scaling of the discharges compared to the ITER baseline and hybrid scenarios, but this goes outside the scope of this paper. Table 1 summarizes the main plasma parameters of the discharges from the multimachine database used for the pedestal studies in this paper. FIG. 1 illustrates the datasets for each tokamak, in terms of H98(y,2) and density variation.

Table 1. Main plasma parameters of the discharges from the multimachine database.

tokamak	scenario	Ip[MA]	ne[10^{19} m^{-3}]	q95	δ	β_N	li	P_{NET}[MW]
AUG	**Standard H-modes**	0.8 1.0	$5.0 - 6.7$ $4.7 - 6.7$	$3.7 - 5.1$ $3.2 - 4.4$	0.14-0.44 0.13-0.34	$1.3 - 2.5$ $1.3 - 2.3$	$0.8 - 1.0$ $0.9 - 1.0$	$4.0 - 8.0$ $4.4 - 5.8$
	Improved H-modes	0.8 1.0	$5.3 - 5.9$ $4.9 - 6.0$	4.8 4.6	0.22-0.26	$1.7 - 3.0$ $1.9 - 3.0$	$0.8 - 0.9$ $0.8 - 1.0$	$5.0 - 11.1$ $7.5 - 11.8$
DIII-D	**Standard H-modes**	1.2	$6.4 - 10.0$ ~ 6.0	4.3 4.2	0.3 0.5	$1.6 - 2.0$ $1.9 - 2.3$	$0.9 - 1.1$	$3.5 - 7.2$ $3.6 - 6.7$
	Hybrid discharges	1.2	~ 5.0	$4.2 - 4.5$	0.5	$2.0 - 3.2$	$0.8 - 0.9$	$4.5 - 9.2$
JET	**Standard H-modes**	2.0 2.5	$4.8 - 5.6$ $6.3 - 8.0$	$3.6 - 3.8$ $3.0 - 4.6$	$0.25 - 0.43$ 0.43	$1.4 - 2.0$ $1.3 - 2.0$	$0.9 - 1.0$ $0.8 - 0.9$	$10.3 - 17.8$ $14.4 - 17.5$
	Hybrid discharges	1.4 2.0	$2.1 - 3.8$ $3.1 - 5.6$	$3.5 - 4.1$ $3.8 - 4.0$	0.22, 0.45 0.21, 0.42	$2.0 - 2.7$ $1.9 - 2.4$	$0.7 - 0.8$ $0.7 - 0.8$	$8.7 - 17.6$ $15.8 - 21.2$
JT-60U	**Standard H-modes**	1.0 1.8	$1.5 - 3.8$ $3.4 - 4.0$	$3.0 - 5.3$ 3.1	$0.13 - 0.49$ 0.26	$1.1 - 2.5$ $1.0 - 1.3$	$0.8 - 1.1$ $0.9 - 1.0$	$5.1 - 10.9$ $10.7 - 14.2$
	High βpol H-modes	1.0 1.8	$2.0 - 3.5$ $3.3 - 4.0$	3.3-5.2;6.5 3.1; 4.0	0.27; 0.47 0.27; 0.34	$1.0 - 2.7$ 1.2; 2.1	1.0; 0.5-0.8 $0.9 - 1.0$	$6.6 - 20.7$ 13.0; 22.0
	RS H-modes	$0.8 - 1.0$	$1.8 - 2.8$	$6.5 - 9.0$	$0.38 - 0.47$	$1.2 - 2.1$	$0.6 - 0.8$	$5.0 - 7.7$

The AUG discharges were selected from the AUG pedestal database, namely the ELMy H-modes with the best pedestal measurements (see section 3) and therefore are not representative of the best performance discharges from AUG. The improved H-modes include discharges with early (IH early heat.) and late heating (IH late heat.) [9,10]. For DIII-D, standard H-modes and

hybrid discharges at 1.2 MA were selected. Operationally there is a separation in density between the hybrids and the conventional H-modes, with the hybrid discharges run at low density. Nonetheless, a significant variation in confinement is found in the hybrid data at roughly constant density. For JET, standard H-modes were selected from [11,12] and the hybrid discharges from the JET hybrid experiments [6], based on the availability of both Ti and Te profiles (see section 3) . For JT-60U, conventional type I ELMy H-modes were obtained in series of H-mode experiments [13, 14, 15]. Some of these discharges have weak internal transport barriers (ITBs) and are labelled as "high β_{pol} H-mode" here. In contrast to these standard H-modes, "high β_{pol} H-modes" and "RS H-modes" have ITBs, with positive and negative shear, respectively. Quasi-steady high β_{pol} H-modes [16] with the current profile near its steady-state value and quasi-steady RS H-modes [8], [17] with a large bootstrap current fraction are selected here.

3. Pedestal measurements and analysis techniques

The pedestal top pressure is the most accessible parameter and can be measured in all four tokamaks. In this paper, we study both electron and ion pedestal pressures. For AUG, edge Te and ne profiles were obtained from the high resolution edge diagnostics, as explained in detail in [18]. A composite profile was generated from all profiles collected within the selected stationary time window and then fit by a modified hyperbolic tangent function [19], [20], which joins a polynomial function in the core and one in the scrape-off-layer. At present, high resolution measurements of the ion edge transport barrier (ETB) are not possible on a routine basis in AUG. For the AUG discharges analysed in this paper, the pedestal top ion temperature (Ti^{PED}) was thus obtained by fitting the Ti profile measured by core CXRS imposing a fixed pedestal width and radial position for the ion ETB, using a similar fitting function as that for the edge electron profiles. This carries some uncertainty in the determination of Ti^{PED} and, therefore, of pi^{PED}. For the evaluation of the contribution of the pedestal to the global confinement the pedestal top parameters are deduced from the profile fits to data from all phases of the ELM cycle (ELM-averaged technique). For one AUG case, we have fitted separately the edge profiles during one ELM cycle (one profile every 1 ms) and then taken the time average of the pedestal top values. The two analysis techniques yielded very similar pedestal top values for this test case. For DIII-D, the Te and ne profiles were measured by a multiple-point TS system and composite profiles were obtained in the time window of interest. Laser pulses which were close to ELMs were removed by an ELM detection scheme based on the use
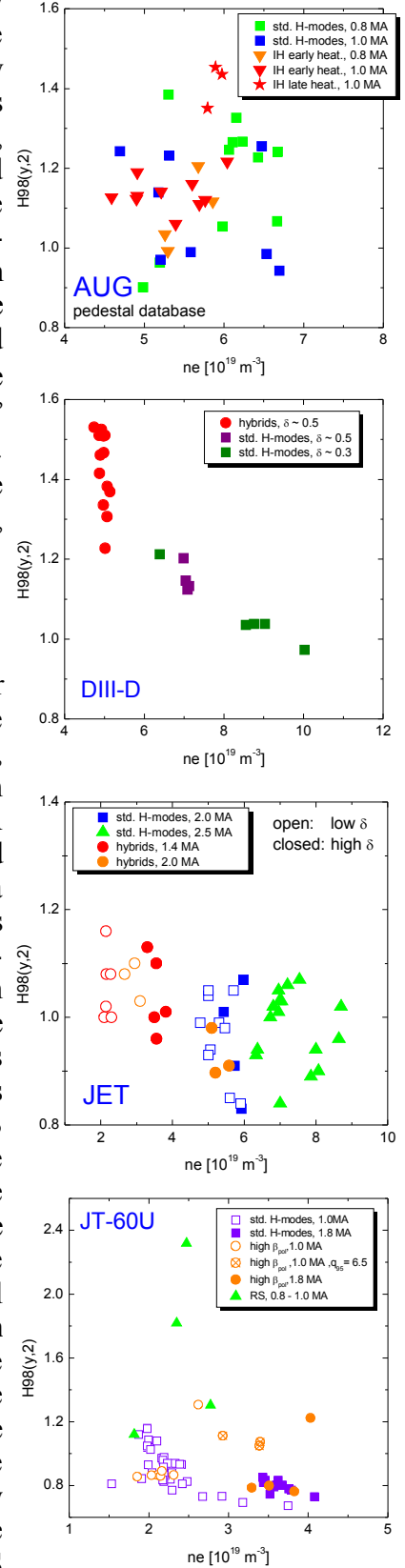

FIG. 1. *H98(y,2) vs line averaged density for AUG, DIII-D, JET and JT-60U.*

of D-alpha signals. The Te and ne data were fit in the same way as for the AUG profiles. The ion temperature and carbon density were obtained from CXRS and the Ti profiles were fit in a similar way as for the electron profiles. In JET the electron temperature pedestal top value (Te^{PED}) is determined at the radial position where the Te profile measured by the ECE radiometer changes slope. Lacking profile information, the electron density pedestal top (ne^{PED}) is assumed to be equal to the line averaged density measured by the edge channel of the FIR interferometer. The Ti profile is obtained by combining core and edge CXRS Ti profiles. Since the spatial resolution of the edge CXRS system does not allow for unambiguous determination of Ti^{PED}, this was assumed to be equal to the value of the Ti profile at the same radial position as Te^{PED}. This can lead to an uncertainty of at least 20% in the value of Ti^{PED}. The pedestal top values are the average of the corresponding quantities over the chosen stationary time window. In JT-60U the Te and ne profiles were obtained from TS measurements. Electron profiles for the experiments in [15] were taken at one time slice between (or just before) ELMs, and those for other experiments were averaged over several laser pulses. The Ti profiles were measured by a combination of core and edge CXRS and are ELM-averaged. The pedestal top electron temperature and density and ion temperature were obtained by bilinear fits of the respective profiles. The total pedestal top pressure is calculated as $p^{PED} = p_e^{PED} + p_I^{PED}$, where $p_e^{PED} = n_e^{PED} \times T_e^{PED} \times e$ and $p_I^{PED} = n_I^{PED} \times T_i^{PED} \times e$, where nI is the sum of the deuteron and impurity ions density. For DIII-D n_I^{PED} is calculated from ΔZ_{eff} from CXRS and for JET and JT-60U n_I^{PED} is calculated from Z_{eff} measured by visible bremsstrahlung, assuming that carbon is the dominant impurity. In AUG, for the standard H-modes we have assumed an average carbon concentration of 1.5% and an average helium concentration of 10% (due to frequent glow discharge cleaning in between plasma discharges), while for the improved H-modes the impurity densities of the main intrinsic impurities have been measured by CXRS.

4. Power dependence of pedestal parameters
4.1. Power dependence of pedestal top pressure

FIG. 2 shows the variation of p^{PED} with P_{NET} in the 4 tokamaks, where the discharges are grouped by plasma current, shape and operating mode. In order to guide the eye, curves of $p^{PED} \sim P_{NET}^{0.31}$ (i.e. following the power scaling of the IPB98y2 H-mode confinement scaling) have been added for each plasma current. There is a general trend in all tokamaks for p^{PED} to increase with input power along this curve for most of the discharges at a given Ip. Compared to this trend, higher pedestal pressures are found in AUG in improved H-modes
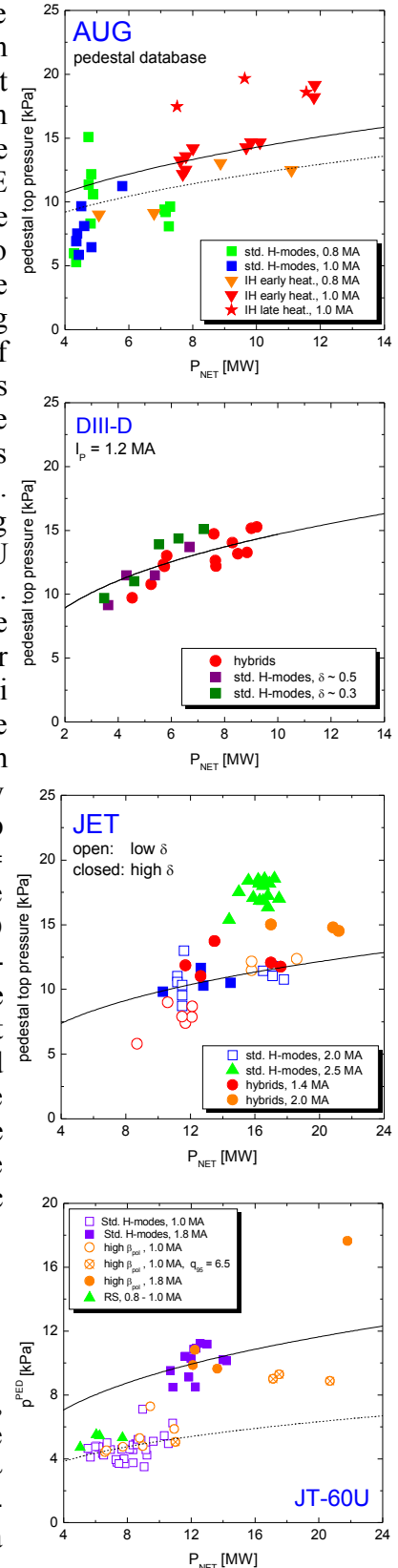

FIG. 2. *p^{PED} vs. P_{NET}. The lines are to guide the eye only along the curve $p^{PED} \sim P_{NET}^{0.31}$.*

with late heating and with early heating at 12 MW and in JT-60U for the high β_{pol} discharges at $q_{95} = 6.5$ and high δ. Characteristics specific to each machine are also observed. In AUG standard H-modes at 0.8 MA there is a significant variation of p^{PED} with P_{NET}, due to variations in plasma shape. Part of the scatter may also be due to the uncertainties in pi^{PED}. In the improved H-modes with late heating Te^{PED} is typically higher than in the early heating counterpart and the ETB stored energy is essentially constant with input power. In DIII-D p^{PED} increases with P_{NET} in a similar fashion both for the standard H-modes and the hybrid discharges analysed. For the standard H-modes at low δ part of the increase in p^{PED} with power is due to an increase with density, since density and power variation are coupled for this group of discharges. In JET, also due to uncertainties in pi^{PED} there is a comparatively large scatter in p^{PED}, so that it is not possible to separate the increase of p^{PED} with Ip from that with P_{NET} at 1.4 and 2 MA in this dataset. The pedestal pressure increases with power roughly in the same way in the standard H-modes and in the hybrid discharges. In the hybrid discharges the input power is correlated to the plasma triangularity. The conventional H-modes at 2.5 MA do not cover a sufficiently broad power range in order to determine trends, but are plotted for comparison. In JT-60U, the pedestal pressure in RS H-modes varies with input power in a similar way as the standard H-modes and high β_{pol} discharges at low q_{95} at 1 MA.

4.2. Power dependence of ETB widths

In order to reduce the scatter due to ELMs in the measurement of the widths and gradients of the ETB region, in AUG an ELM-syncronized analysis of the edge profiles is performed [20]. The edge profiles are first averaged over short time windows (typically 2-3 ms) during the ELM rise period, equidistant from each ELM and then averaged over the stationary time window of interest. Using this technique, it is found that as P_{NET} is increased in the improved H-modes power scan the width of the density ETB (Δne) stays roughly constant, whereas the Te ETB (ΔTe) broadens with power. ne^{PED} tends to increase with power (in the absence of gas fuelling) due to a combination of steepening of the density gradient in the ETB and of increasing density in the scrape-off-layer, which raises the base level of the density barrier [21]. Te^{PED} also increases with power, due to an increase of the width of the temperature ETB. At high power Δne is narrower than ΔTe, with $\Delta ne \sim 1$ cm and $2 < \Delta Te < 3$ cm (FIG. 3), in contrast to previous analysis on lower power conventional H-modes [20]. With late heating, Δne and ΔTe are similar to those measured with early heating. In DIII-D, the density ETB is broader and the density gradient is less steep for hybrid discharges than for standard H-mode discharges. Since both the input power and the density are systematically different in these datasets, it is not possible to conclude whether this is a power or a density effect (or a combination of the two). The Te and Ti ETBs broaden with input power in a continuous way from conventional H-modes to hybrid discharges. The widths of the ne and Te ETB's are of comparable magnitude, with $1 < \Delta ne \sim \Delta Te < 3$ cm, while the ion temperature pedestal is much broader at high power, with an overall variation of $2 < \Delta Ti < 7$ cm. At high power, a steepening of the Ti gradient in the ETB is also observed. Therefore, the increase of pi^{PED} at high power is due to an increase of both width and gradient of the Ti ETB. The increase in pe^{PED} at high power, instead, is due solely to an increase in width of the Te ETB. Based on these results, we could speculate that at high power the total pedestal pressure in AUG and JET might be underestimated in our study due to the assumption of $\Delta Te = \Delta Ti$ made in the previous section.
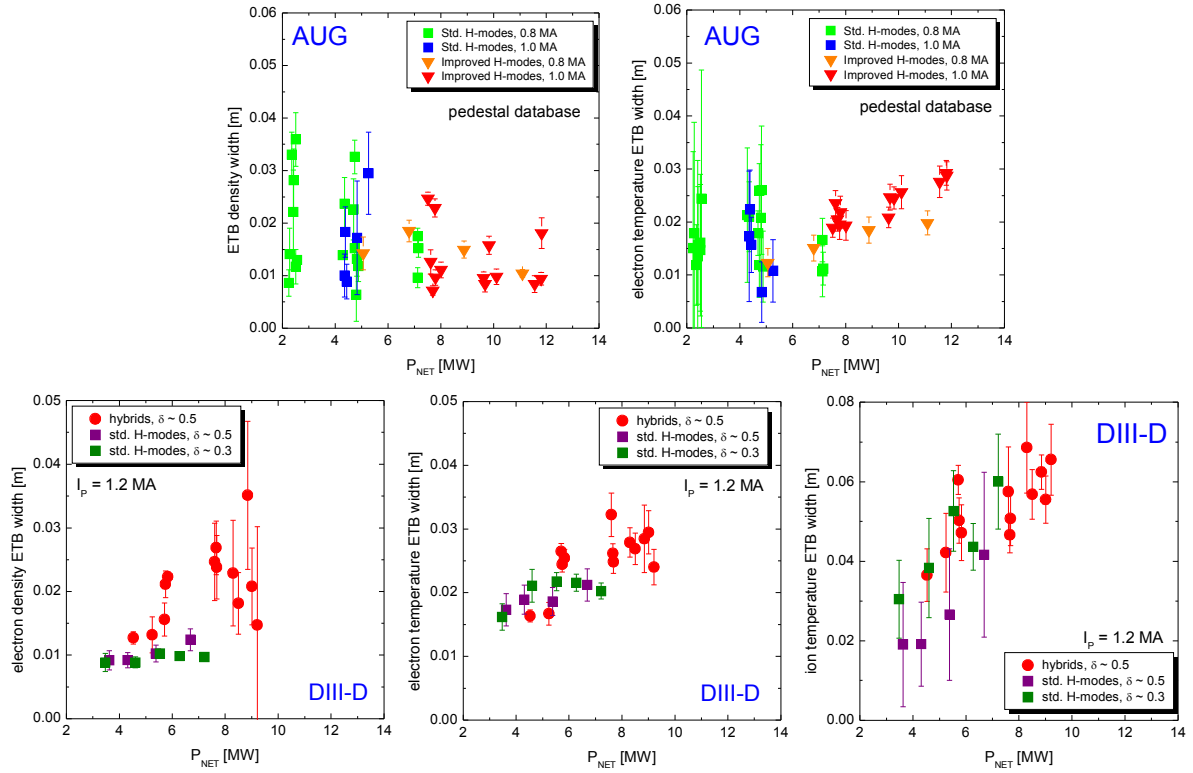
FIG. 3. *ne and Te ETB widths (AUG) and ne, Te and Ti ETB widths (DIII-D) versus P_{NET}.*

5. Relation between pedestal and global confinement and stability

We define the total thermal stored energy $W_{th} = W_{core} + W_{PED}$, with $W_{PED} = 3/2$ p^{PED} x Vol, where Vol is the total plasma volume. FIG. 4 shows that at a given plasma current Wth also increases with input power roughly as $P_{NET}^{0.31}$ for all tokamaks for most discharges. Higher stored energies compared to this trend are found in AUG for the improved H-modes with late heating and for the improved H-modes with early heating at the highest power, in DIII-D for the hybrid discharges at high power and in JT-60U for the high β_{pol} discharges at $q_{95} = 6.5$ and for the RS H-modes. In JET no significant difference between standard H-modes and hybrid discharges is observed in terms of power variation of Wth. From FIG. 5 and FIG. 3 it can be seen that the confinement improvement obtained at high input power is due to an increase of both pedestal and core stored energy in AUG improved H-modes, while it is primarily due to improved core confinement in DIII-D hybrid discharges. In JT-60U RS H-modes W_{core} increases significantly at fixed W_{PED}, showing decoupling of W_{core} from W_{PED} in the presence of strong ITB's. Instead, for the high β_{pol} H-modes at $q_{95} = 6.5$, the increase in Wth is due to an increase of W_{PED} with power at constant W_{core}. In the JET hybrid discharges at 1.4 MA, Wth increases with power and triangularity due to an increase of W_{PED}. For the remaining dataset, a significant variation in W_{core} is found at similar values of W_{PED} due to variations in density, safety factor and triangularity and the overall increase of W_{core} with W_{PED} is clearly driven by the increase in Ip. Finally, in FIG. 6 (a) and (b) we analyse our multimachine database in terms of normalized parameters. For JT-60U it has been shown [22] that in type I ELMy discharges the pedestal β_{pol} is a measure for edge stability and that both energy confinement factor and total normalized pressure increase with improved edge stability for type I ELMy H-modes with and without ITBs [23]. Similar studies have also been reported for DIII-D [24]. For all four tokamaks it can be seen that the pedestal β_{pol} increases with the total β_{pol}. This indicates either that improved

edge stability is due to increased Shafranov shift or that increased pedestal stored energy leads to increased total stored energy through teperature profile stiffness, in the absence of ITBs. While AUG, DIII-D and JET are aligned along a similar slope, for JT-60U most of the increase in total β_{pol} is sustained by core pressure, except for the high β_{pol} discharges at high q_{95}. It is however not possible to determine at this stage whether an increase in total β_{pol} drives an improvement in edge stability or vice versa. FIG. 6 (b) shows that there is also a general trend for H98(y,2) to increase with pedestal β_{pol}. In addition, in each tokamak a variation in H98(y,2) at constant pedestal β_{pol} is observed. For JT-60U the weaker role of the edge stability is compensated by the core in the energy confinement factor, since there is no clear separation amongst the four tokamaks in terms of H98(y,2) versus pedestal β_{pol}.

6. Conclusions

In this paper we have compared pedestal and global parameters in ELMy H-mode discharges with varying input power and current profiles from AUG, DIII-D, JET and JT-60U. In particular, both electron and ion pedestal pressures have been studied. The transition from "standard H-modes" to improved confinement scenarios is continuous with increasing input power, with overlap in the operating space. Based on physics analysis rather than "control room labels" some of the discharges analysed in the paper would be labelled differently. This study shows that the variation of the pedestal parameters is continuous as the input power is increased from standard H-modes to improved confinement scenarios. Compared to the general trend, at the highest input powers higher pedestal pressures are found in AUG improved H-modes and in JT-60U high β_{pol} discharges at $q_{95} = 6.5$ and high δ. Analysis of the pedestal structure shows that in AUG improved H-modes p^{PED} increases with power due to an increase of both n_e^{PED} (steepening of the density gradient in the ETB and of increasing density in the SOL, which raises the base level of the density barrier) and T_e^{PED} (increase of the width of the temperature ETB). In DIII-D p^{PED} increases primarily due to an increase of the pedestal temperature via an increase in width of the T_e ETB and an increase of both width and gradient of the T_i ETB. For AUG improved H-modes the confinement improvement obtained at high input power is due both to an increase in W_{PED} and in W_{core}, while in DIII-D hybrid discharges it is primarily due to an increase in W_{core}. In JT-60U high β_{pol} H-modes at $q_{95} = 6.5$ and high δ the improved confinement at high power is due to an increase of W_{PED} with power at constant W_{core}. In JET hybrid discharges at 1.4 MA W_{th} increases with power and triangularity due to an increase
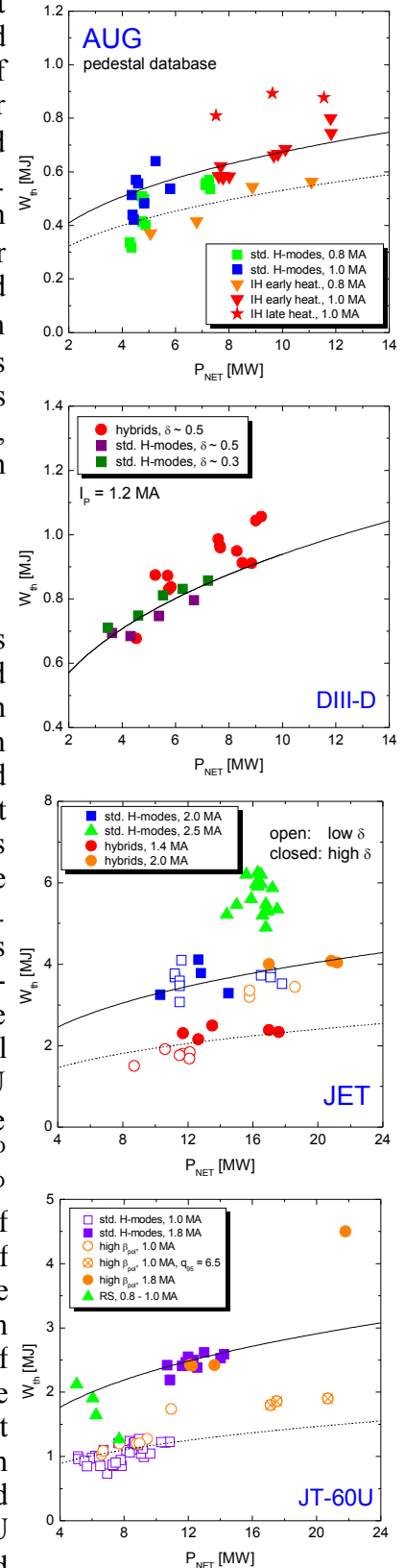

FIG. 4. W_{th} vs. P_{NET}. The lines are to guide to the eye only along the curve $W_{th} \sim P_{NET}^{0.31}$.

of W_{PED}. For all four tokamaks there is a correlation between pedestal β_{pol} (edge stability) and total β_{pol}. While AUG, DIII-D and JET are aligned along a similar slope, for JT-60U most of the increase in total β_{pol} is sustained by core pressure, except for the high β_{pol} discharges at high q_{95} and triangularity. It is however not possible to determine whether an increase in total β_{pol} drives an improvement in edge stability or viceversa. A general trend for H98(y,2) to increase with pedestal β_{pol} is also observed, although with variations in H98(y,2) at constant pedestal β_{pol} in each machine.

References:
[1] ITER Physics Basis, Nucl. Fusion **39** (1999) 2137.
[2] McDONALD, D.C. et al., this Conference, EX/P3-5.
[3] GRUBER, O., et al., Phys Rev. Lett. **83** (1999) 1787.
[4] SIPS, A.C.C., et al., Plasma Phys. Control. Fusion **44** (2002) A151.
[5] WADE, M.R., et al., Nucl. Fusion **45** (2005) 407.
[6] JOFFRIN, E., et al., Nucl. Fusion **45** (2005) 626.
[7] KAMADA, Y. and JT-60U TEAM, Nucl. Fusion **41** (2001) 1311.
[8] FUJITA, T., et al., Phys. Rev. Lett. **87** (2001) 085001.
[9] STOBER, J.K. et al., this Conference, EX/P1-7.
[10] SIPS, A.C.C. et al., this Conference, EX/1-1.
[11] SARTORI, R., et al., Proc. 20th IAEA Conf. Vilamoura, 2004, EX/6-3.
[12] SARTORI, R., et al., H-mode workshop 2005.
[13] URANO, H., et a l., Plasma Phys. Control. Fusion **44** (2002) 11.
[14] URANO, H., et al., Plasma Phys. Control. Fusion **46** (2006) A193.
[15] SAIBENE, G., et al., Proc. 20th IAEA Conf. Vilamoura, 2004, IT/1-2
[16] KAMADA, Y., et al., Plasma Phys. Control. Fusion **44** (2002) A279.
[17] FUJITA, T., et al., Nucl. Fusion **42** (2002) 180.
[18] SUTTROP, W., et al., this Conference, EX/P8-5.
[19] GROEBNER, R.G. et al., Phys. Plasmas **5** (1998) 1800.
[20] HORTON, L.D., et al., Nucl. Fusion **45** (2005) 856.
[21] HORTON, L.D., et al., Proc. EPS Conf. 2006, Rome, Italy.
[22] KAMADA, Y., et al., Plasma Phys. Control. Fusion **44** (2002) A279.
[23] KAMADA, Y., et al., Plasma Phys. Control. Fusion **48** (2006) A419.
[24] GROEBNER, R.J., et al., Plasma Phys. Control. Fusion **48** (2006) A109.

*See the Appendix of M.L. Watkins et al., Fusion Energy 2006 (Proc. 21st Int. Conf. Chengdu, 2006) IAEA, 2006.

FIG. 5. Wcore vs. W_{PED}.

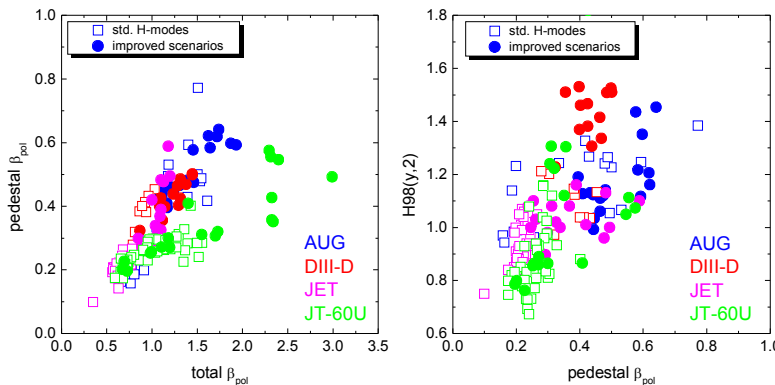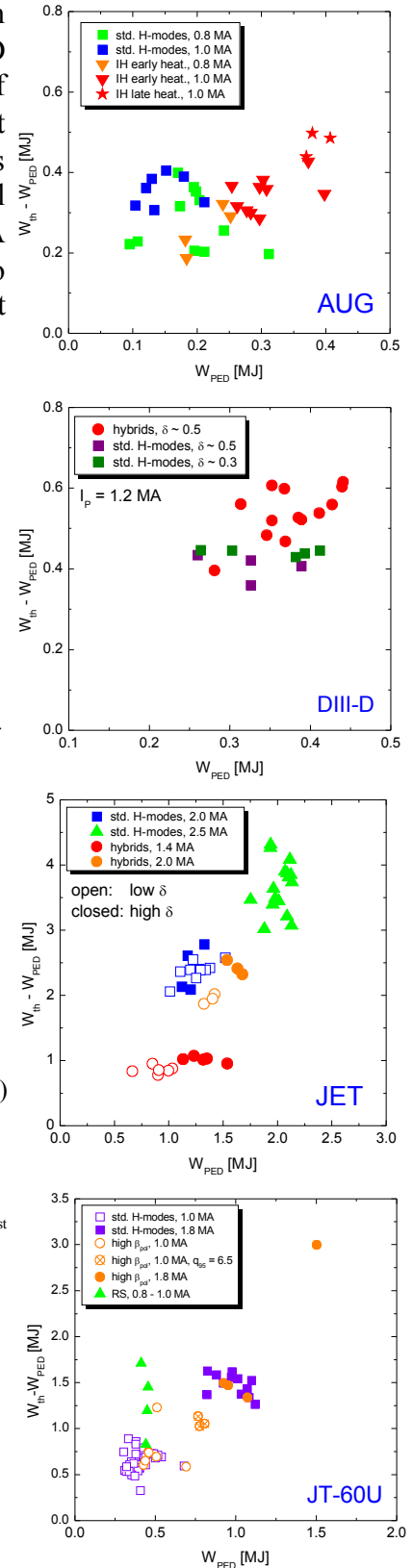**FIG. 6.** Pedestal β_{pol} vs total β_{pol} (a) and H98(y,2) vs pedestal β_{pol} (b).